Top Catal (2009) 52:1746–1751
DOI 10.1007/s11244-009-9342-x

ORIGINAL PAPER

Influence of Pt–Ba Proximity on NO_x Storage–Reduction Mechanisms: A Space- and Time-Resolved In Situ Infrared Spectroscopic Study

Nobutaka Maeda · Atsushi Urakawa · Alfons Baiker

Published online: 15 July 2009

Abstract The influence of Pt–Ba proximity on the performance and mechanism of NO_x storage–reduction (NSR) was investigated by a comparative study of Pt–Ba/CeO_2, Pt/CeO_2 and mechanically mixed Pt/CeO_2–Ba/CeO_2. NO_x storage capacity, regeneration activity and selectivity to nitrogen and ammonia during periodic lean (NO + O_2)–rich (H_2) cycles were evaluated and the chemical gradients along the axial direction of the catalyst beds were monitored by space- and time-resolved in situ diffuse reflectance infrared Fourier transform spectroscopy (DRIFTS). The presence of Ba and its proximity to Pt greatly influenced the NSR process. In particular, the proximity was crucial to achieve better utilization of bulk Ba components as well as enhancing selectivity to N_2. The space-resolved approach is shown to be a powerful tool to understand the impact of the proximity of Pt and Ba constituents on the final NSR performance.

Keywords NO_x storage–reduction · Pt–Ba proximity · Mechanically mixed catalyst · In situ spectroscopy · Space- and time-resolution

1 Introduction

NO_x storage–reduction (NSR) is one of the key technologies to reduce NO_x emissions from vehicles under oxygen-rich conditions [1–3]. Generally, NSR catalysts consist of metal oxides such as Al_2O_3 and CeO_2 as supports, on which a noble metal (usually Pt) is finely dispersed together with a storage component consisting of an alkali or an alkaline-earth metal component (usually Ba). During the fuel-lean phase (ca. 1 min), NO is oxidized to NO_2 on Pt, and the produced NO_2 is subsequently stored by the Ba components as $Ba(NO_3)_2$. During the short fuel-rich phase (3–5 s), stored NO_x is released and reduced on the metal component (Pt) by hydrocarbons, CO and H_2. A commonly accepted feature of the NO_x storage mechanism is that Ba nitrites are first formed by the reaction of barium oxides and/or hydroxides with NO_2 and then slowly oxidized to Ba nitrates [3]. Under rich conditions, a two-step NO_x reduction mechanism has been recently proposed; the formation of ammonia by the reaction of nitrates with H_2, and the subsequent reduction of residual Ba nitrates by the produced ammonia [4]. The propagation of NSR progresses from the upstream to downstream position of catalyst beds as well as the sequential nature of both storage and reduction processes result in drastic gradients of chemical species on the surface and in the bulk of catalyst, particularly in the axial direction of the catalyst bed. The spatially resolved monitoring of concentration gradients of nitrate species over Pt–Ba/Al_2O_3 monolithic catalysts revealed that NO_2, which was formed via NO oxidation at the inlet, was stored at the downstream position during lean periods [5]. We have recently reported the monitoring of dynamic surface-bulk NSR processes along a Pt–Ba/CeO_2 catalyst bed by means of combined space- and time-resolved DRIFT (diffuse reflectance infrared Fourier transform) and Raman spectroscopy [6]. The combined approach elucidated the position-dependent bulk utilization of the storage component under lean conditions and the evolution of bulk Ba hydroxides under rich conditions. The different local sensitivity between DRIFTS

N. Maeda · A. Urakawa (✉) · A. Baiker (✉)
Department of Chemistry and Applied Biosciences, Institute for Chemical and Bioengineering, ETH Zurich, Hönggerberg, HCI, 8093 Zurich, Switzerland
e-mail: urakawa@chem.ethz.ch

A. Baiker
e-mail: baiker@chem.ethz.ch

(surface-sensitive) [7] and Raman spectroscopy (bulk-sensitive) [8] allowed discrimination between surface and bulk chemical processes, which indicated that Ba nitrites were merely a surface intermediate that underwent further oxidation to produce surface nitrates and bulk nitrates.

In spite of a number of studies devoted to the deeper understanding of mechanistic aspects, the importance of Pt–Ba proximity on the NSR catalyst is still poorly understood. In particular, its influence on the chemical gradients along the catalyst bed has not been investigated. Pt–Ba location is considered to be of pivotal importance to realise efficient NO_x storage and catalyst regeneration via spillover processes of reaction intermediates between Pt and Ba [9]. Several groups reported the comparative study of Pt–Ba/Al_2O_3 and a physical mixture of Pt/Al_2O_3 and Ba/Al_2O_3, where Pt and Ba constituents were spatially separated, hindering the spillover process [10–13]. The results of these studies indicated that Pt affects the rate of nitrate decomposition only if Pt and Ba are dispersed on the same alumina particles. In this contribution, we investigate the importance and relevance of Pt–Ba proximity on the overall NSR mechanism and performance using three types of ceria supported catalysts, Pt–Ba/CeO_2, a mechanical mixture of Pt/CeO_2 and Ba/CeO_2, and Pt/CeO_2, by in situ space- and time- resolved DRIFTS.

2 Experimental

The catalysts were prepared by incipient wetness impregnation of the aqueous solution of a platinum precursor (diammineplatinum (II) nitrite) and/or a barium precursor ($Ba(NO_3)_2$) to obtain 1 wt% Pt and 20 wt% Ba on a ceria support with respect to the catalyst weight after calcination. Detailed information of used chemicals and of the catalyst preparation procedure has been given elsewhere [6]. Mechanically mixed Pt/CeO_2–Ba/CeO_2 was prepared by mixing the respective components in an agate mortar. After impregnation, the samples were dried overnight at 353 K and then calcined in air at 773 K for 3 h.

NSR measurements were carried out with 100 mg of catalyst in a plug-flow cell designed for in situ DRIFT-Raman spectroscopic studies with μm-space (positioning) and ms-time resolution [6, 14]. The concentrations of the effluent gas were monitored by a chemiluminescence detector (ECO PHYSICS, CLD 822 S) and a mass spectrometer (PFEIFFER VACUUM, THERMOSTAR^{TM}). Prior to NSR measurements, the fresh catalysts were reduced by hydrogen (3.3% H_2 in balance He) at 623 K for 1 h, and then exposed to several lean (0.42 vol% NO, 3.3 vol% O_2, balance He)–rich (3.3 vol% H_2, balance He) cycles at 623 K (both 211 s at 60 mL/min, space velocity: 37,500 h^{-1}) until a reproducible concentration response of effluent gas components was attained.

3 Results and Discussion

Figure 1 shows the evolution of NO_x concentrations (A, D, G), selected gaseous components (B, E, H), and DRIFT spectra (C, F, I) during NSR over Pt–Ba/CeO_2 (A–C), mechanically mixed Pt/CeO_2–Ba/CeO_2 (D–F) and Pt/CeO_2 (G–I). Pt–Ba/CeO_2 stored a large amount of NO (ca. 3,700 ppm) steadily throughout lean periods (Fig. 1A), achieving 85.7% NO conversion. NO_2 evolution in the effluent stream was almost negligible, implying that all the NO_2 produced via oxidation of NO over Pt surfaces was successfully captured by the Ba components and ceria support. Pt/CeO_2–Ba/CeO_2 exhibited less NO_x storage (NO conversion 39.0%) and considerable NO_2 and NH_3 formation, leading to lower reduction selectivity to N_2 (Fig. 1D). NH_3 formation during rich periods was observed after that of N_2. It should be noted that the Pt/CeO_2–Ba/CeO_2 was prepared by mixing Pt/CeO_2 and Ba/CeO_2 which have the same loading as the Pt–Ba/CeO_2 with respect to the ceria support and dispersion of Ba species similar to that of Pt–Ba/CeO_2; therefore the actual loading of Pt and Ba in Pt/CeO_2–Ba/CeO_2 is half of that in Pt–Ba/CeO_2. Still, the effective storage capacity was less than half, clearly indicating that the Pt–Ba proximity influences the NO_x storage capacity. Moreover, the NO conversion of 39% would be not doubled when doubling the catalyst amount, due to different degree of utilization of catalyst along the axial direction of the catalyst bed as will be shown later. The NSR performance of Pt/CeO_2 was surprisingly high (Fig. 1G), showing 48% NO conversion without producing NH_3. NO and a remarkable amount of NO_2 evolved, which gradually increased during the lean periods. In all three catalytic systems, a sharp spike of NO_x release was detected when the gas-flow was switched to the rich condition, likely due to stronger interaction of formed water with the support [6, 15], less stability of surface-adsorbed NO_x induced by the atmosphere change [16] and exothermicity of the reduction [5].

Comparison of H_2, H_2O, N_2, and O_2 evolution profiles in the effluent streams (Fig. 1B, E, H) shows similar trends although the absolute concentrations considerably differ. The major difference is the evolution of H_2O for Pt–Ba/CeO_2. The H_2O formation ceased when no more H_2 was consumed for NO_x reduction for Pt/CeO_2–Ba/CeO_2 and Pt/CeO_2, while Pt–Ba/CeO_2 showed a steadily increasing H_2O formation even after NO_x reduction had been completed (as observed by N_2 decrease and H_2 increase). H_2O formation then suddenly dropped at ca. 410 s. Interestingly, the H_2O profile did not correlate with those of the other gas components. NO_x reduction has been reported to involve

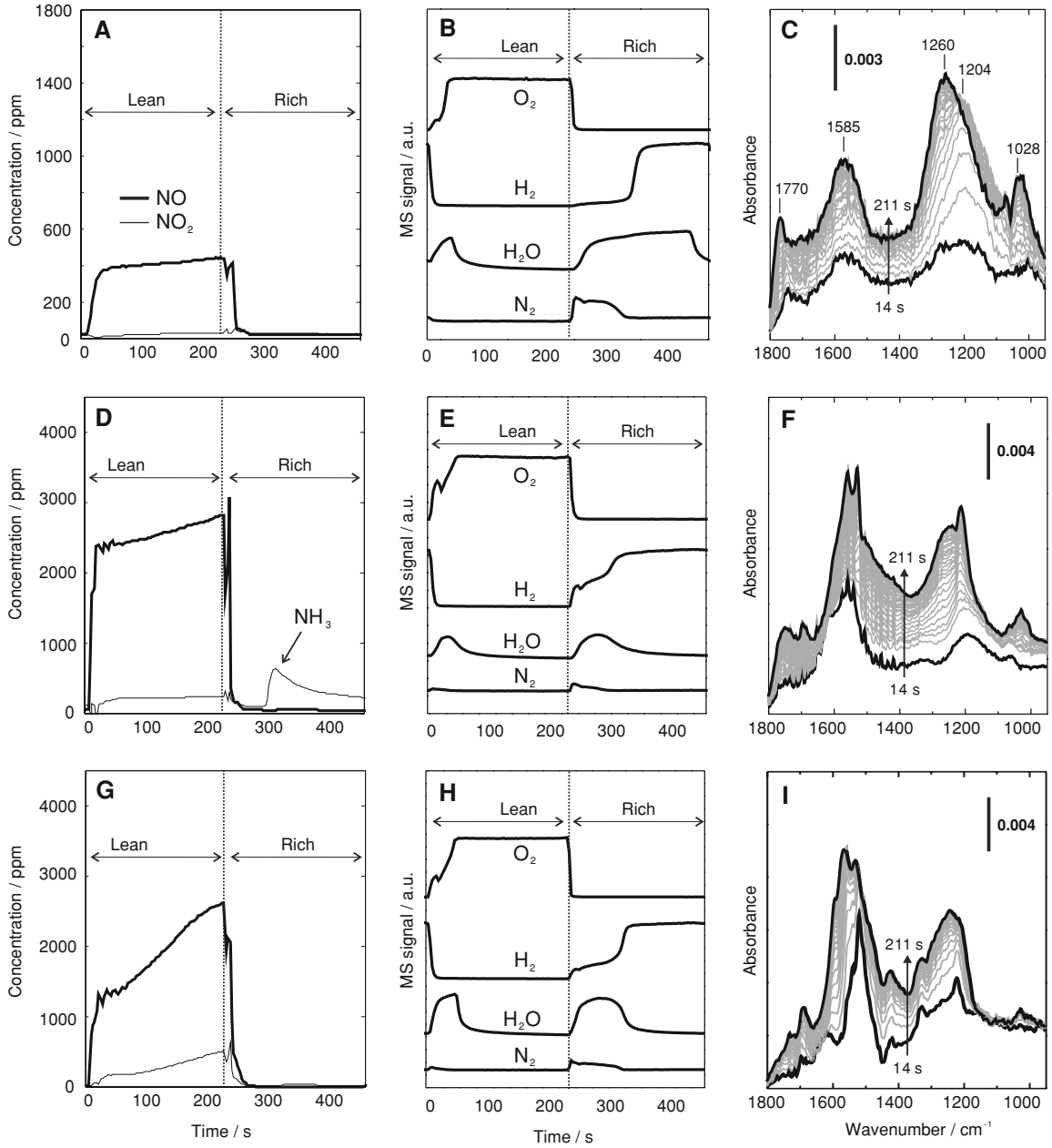

Fig. 1 **A**, **D**, **G** NO_x concentrations, **B**, **E**, **H** gas-phase compositions, and **C**, **F**, **I** DRIFT spectra during lean–rich periods over **A**–**C** Pt–Ba/CeO_2, **D**–**F** mechanically mixed Pt/CeO_2–Ba/CeO_2 and **G**–**I** Pt/CeO_2 at 623 K. For **C**, **F**, **I**, the last spectrum of rich periods was used as background

several reaction steps. Recently, Lietti and co-workers reported that the overall H_2 consumption and the formation of NH_3 and N_2 during rich periods were in line with the stoichiometry of the following reactions [4]:

$$Ba(NO_3)_2 + 5H_2 \rightarrow N_2 + Ba(OH)_2 + 4H_2O \quad (1)$$

$$Ba(NO_3)_2 + 8H_2 \rightarrow 2NH_3 + Ba(OH)_2 + 4H_2O \quad (2)$$

$$3Ba(NO_3)_2 + 10NH_3 \rightarrow 8N_2 + 3Ba(OH)_2 + 12H_2O. \quad (3)$$

Our previous Raman spectroscopic study showed the formation of $Ba(OH)_2$, supporting the occurrence of reactions (1–3) where $Ba(OH)_2$ is involved during rich periods. The hydroxide and its hydrate formations may be one of the reasons for the extended H_2O evolution observed for Pt–Ba/CeO_2. However, the consumption of oxygen stored in the ceria support was found to be the predominant process to form H_2O [17]. The NH_3 formation subsequent to N_2 formation observed in this study for Pt/CeO_2–Ba/CeO_2 as well as for Pt–Ba/CeO_2 at a lower temperature (573 K) [6], indicates that reaction (3), the reduction of $Ba(NO_3)_2$ by NH_3, occurs after reaction (2), the NH_3 formation from $Ba(NO_3)_2$ reduction, and that NH_3 is

detected when sufficient $Ba(NO_3)_2$ is not available, especially at the downstream positions of the catalyst bed. As concerns N_2 selectivity, ceria was reported to be highly advantageous compared to the alumina support [18, 19]. This feature has been explained by the possible reaction of NH_3 with oxygen, stored in the ceria, at the downstream position of the catalyst bed [18].

Figure 1C, F, I show time-resolved DRIFT spectra at the front, i.e. upstream position of the catalyst bed during lean periods. IR bands characteristic to Ba species were observed for Pt–Ba/CeO_2 (Fig. 1C). The intense band at 1,204 cm^{-1} is assigned to the ν_3 vibration of nitrites [20–25]. The other bands are assigned to nitrates; the combination mode of $\nu_1 + \nu_4$ of ionic type nitrate at 1,770 cm^{-1} [23, 26], adsorbed bidentate nitrate species[10, 27, 28] at around 1,585 cm^{-1}, and symmetric stretching mode of nitrate [27] at 1,028 cm^{-1}, which is normally infrared inactive unless its structure is distorted. This band is, therefore, assigned to surface nitrates. A band at around 1,260 cm^{-1} also indicates the presence of Ba nitrates. At the beginning of lean periods, the surface bidentate nitrates (1,585 cm^{-1}), and both Ba nitrite (1,204 cm^{-1}) and nitrate (1,260 cm^{-1}) were formed. Subsequently, the transformation of Ba nitrites into ionic Ba nitrates proceeded rapidly, as evidenced by the evolution and the sharpness of bands at 1,770 and 1,260 cm^{-1}. For Pt/CeO_2 (Fig. 1I), all the observed bands are assigned to nitrates adsorbed on the ceria surfaces, i.e. bridging and/or bidentate species [20]. When the Ba species were present near Pt, as in Pt–Ba/CeO_2 (Fig. 1C), the contribution of surface nitrates on the ceria surfaces was not pronounced, and the bands assignable to Ba nitrites and Ba nitrates were intense. Notably, the band characteristics Pt/CeO_2–Ba/CeO_2 (Fig. 1F) resemble those observed for Pt/CeO_2 with some differences due to the contributions from the Ba components (e.g. the bands at 1,260 and 1,770 cm^{-1}). The broad feature of the ionic nitrate band at 1,770 cm^{-1} indicates minor usage of bulk Ba components for NO_x storage. The remarkable differences in the band characteristics between the three catalytic systems underline the important influence of Pt–Ba proximity and consequent differences in the corresponding NSR mechanisms.

We have previously shown that time-resolved vibrational spectroscopy with space-resolution is a powerful tool to investigate gradients of reaction intermediates along catalyst beds and thus provide important insight into catalytic systems where spatial gradients occur [6]. Here we utilize the same technique for the investigation of the effect of the Pt–Ba proximity at three axial positions of the catalyst bed, i.e. front, middle and back positions (0.5, 3.0, 5.5 mm distant from the bed front, respectively; total bed length: 6 mm). Figure 2 shows 2D-surface plots of time-resolved DRIFT spectra during NSR over Pt–Ba/CeO_2 (A–C), Pt/CeO_2-Ba/CeO_2 (D–F) and Pt/CeO_2 (G–I). Over Pt–Ba/CeO_2, NO_x storage occurred mostly at the front position while the contributions of the middle and back positions to the storage process were minor. Compared to Pt–Ba/CeO_2, the NO_x storage at the middle and back positions increased for Pt/CeO_2–Ba/CeO_2, and a totally opposite trend of the gradients, i.e. surface nitrates increase towards the back position, was observed for Pt/CeO_2. The bands of Ba nitrates at 1,260 cm^{-1} and Ba nitrites at 1,204 cm^{-1} were prominent for Pt–Ba/CeO_2 and the band of surface nitrates on the ceria support at 1,560 cm^{-1} was most prominent for Pt/CeO_2. The band characteristics observed for Pt/CeO_2–Ba/CeO_2 (Fig. 2D–F) resemble those of Pt/CeO_2 with significantly less contribution of Ba nitrate and nitrites than for Pt–Ba/CeO_2 as discussed above (Fig. 1F); however the gradient of the stored NO_x was opposite to that of Pt/CeO_2.

Clearly, the proximity of Ba near Pt influences the NO_x storage mechanism and the utilization of the catalyst along the axial direction of the catalyst bed. NO oxidation over Pt and subsequent NO_2 storage occurs most efficiently when Pt and Ba are located closely to each other as in Pt–Ba/CeO_2. This proximity enhances the spillover of NO_x between Pt and Ba over the catalyst surface and hence increases the concentration of surface NO_x near the Ba components. This enhanced spillover most likely results in the utilization of the bulk of the Ba components for NO_x storage as evidenced by the ionic nitrate band at 1,770 cm^{-1} (Fig. 1C). When there are no Ba species present as in Pt/CeO_2, NO_2 produced by NO oxidation over Pt is captured solely by the ceria surface. In this case, the NO_2 concentration is expectedly higher towards the back position, explaining the higher surface nitrate signals over Pt/CeO_2. For the mechanically mixed catalyst, the relatively large distance between Pt and Ba results in hindered spillover processes, therefore decreasing the concentration of NO_2 near the Ba component and storing NO_x species mainly as nitrates on the surfaces of the Ba component as well as on the ceria surface. Still, the presence of the Ba component alters the chemical gradients along the catalyst beds (Fig. 2D–F vs. 2G–I). In this study, NH_3 formation was observed only for the mechanically mixed catalyst. This is also a clear indication that the proximity plays an important role in the efficiency of NO_x reduction; the NH_3 formed from $Ba(NO_3)_2$ and H_2 (reaction 3) was not fully utilized to reduce $Ba(NO_3)_2$ (reaction 3). As a consequence, the selectivity towards N_2 was also improved by the Pt–Ba proximity.

These results suggest that Pt particles have to be located in the vicinity of Ba species in order to optimize the performance of the Ba components as storage materials and also enhance the reduction selectivity to N_2. In addition, the differences in chemical gradients between Pt–Ba/CeO_2

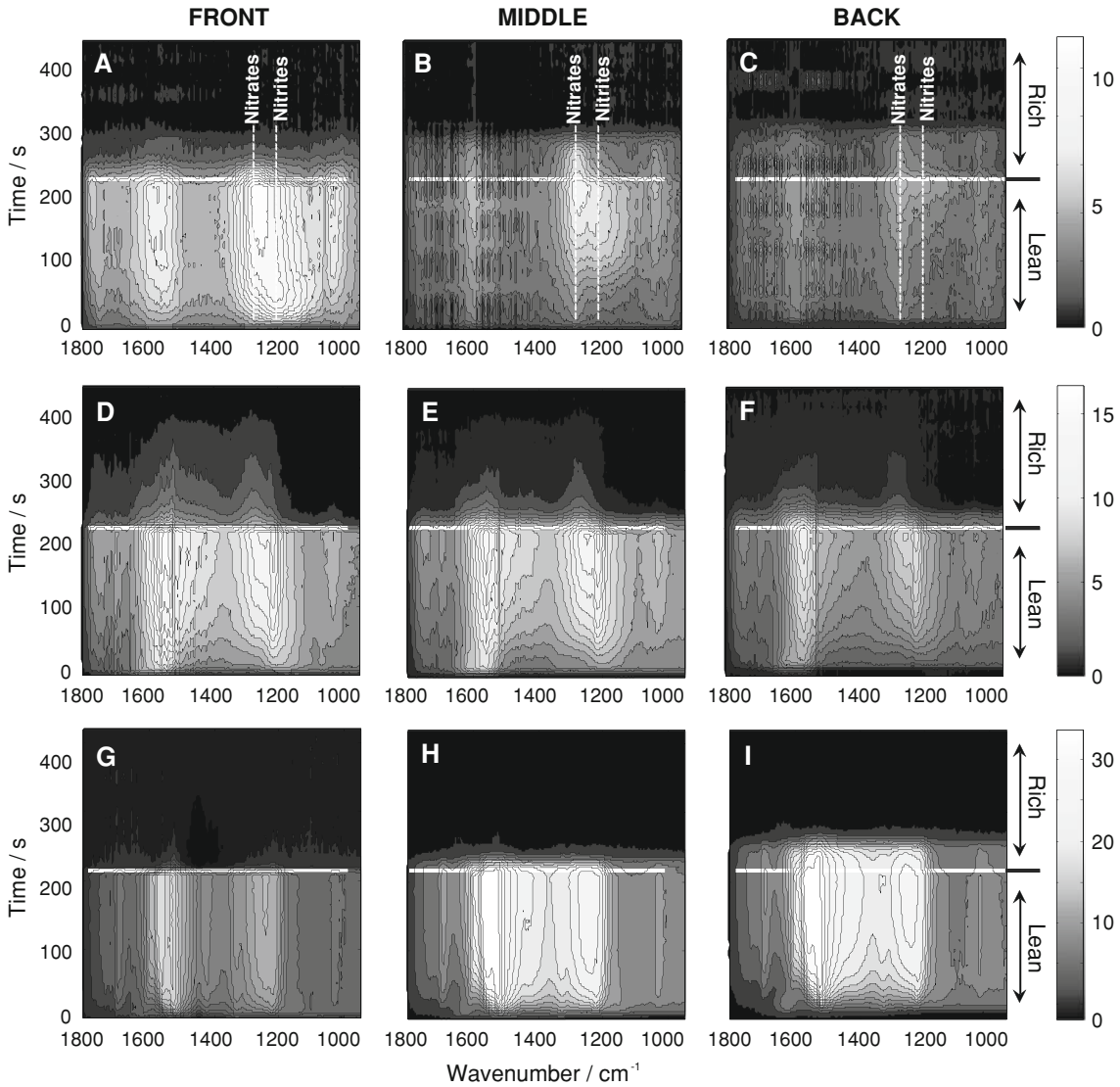

Fig. 2 Time-resolved DRIFT spectra at different positions along the catalyst bed during lean–rich periods over **A–C** Pt–Ba/CeO_2, **D–F** mechanically mixed Pt/CeO_2–Ba/CeO_2 and **G–I** Pt/CeO_2 at 623 K. The units are milli-absorbance. The last spectrum of rich periods was used as background [6]. Copyright Wiley-VCH Verlag GmbH & Co. KGaA. Reproduced with permission

and Pt/CeO_2 also suggest that optimization of the spatial distribution of active components along the catalyst bed could improve the utilization of active components during NSR.

4 Conclusions

The influence of Pt–Ba proximity on NSR was investigated by a comparative study of Pt–Ba/CeO_2, Pt/CeO_2 and mechanically mixed Pt/CeO_2–$BaCeO_2$. NO_x storage capacity, regeneration activity and reaction intermediates were studied by means of temporal analyses of gas-phase composition and DRIFT spectra with space-resolution along the catalyst beds. The presence of Ba and its proximity to Pt strongly influenced the NSR process. Particularly, the proximity was crucial to achieve optimal utilization of bulk Ba components for NO_x storage and high reduction selectivity to N_2. The space-resolved approach offers a powerful opportunity to understand the chemical gradients along the catalyst bed and to design more efficient NSR catalytic systems where the spatial distribution of the key components crucial for storage and catalytic transformations (oxidation/reduction) is optimized.

Acknowledgement Financial support by the Foundation Claude and Giuliana is kindly acknowledged.

References

1. Bögner W, Krämer M, Krutzsch B, Pischinger S, Voigtländer D, Wenninger G, Wirbeleit F, Brogan MS, Brisley RJ, Webster DE (1995) Appl Catal B 7:153
2. Epling WS, Campbell LE, Yezerets A, Currier NW, Parks JE (2004) Catal Rev Sci Eng 46:163
3. Matsumoto SI (2004) Catal Today 90:183
4. Lietti L, Nova I, Forzatti P (2008) J Catal 257:270
5. Aftab K, Mandur J, Budman H, Currier NW, Yezerets A, Epling WS (2008) Catal Lett 125:229
6. Urakawa A, Maeda N, Baiker A (2008) Angew Chem Int Ed 47:9256
7. Roedel E, Urakawa A, Kureti S, Baiker A (2008) Phys Chem Chem Phys 10:6190
8. Harima H (2006) Microelectron Eng 83:126
9. Olsson L, Persson H, Fridell E, Skoglundh M, Andersson B (2001) J Phys Chem B 105:6895
10. Elizundia U, López-Fonseca R, Landa I, Gutiérrez-Ortiz MA, González-Velasco JR (2007) Top Catal 42–43:37
11. Jang BH, Yeon TH, Han HS, Park YK, Yie JE (2001) Catal Lett 77:21
12. Nova I, Lietti L, Castoldi L, Tronconi E, Forzatti P (2006) J Catal 239:244
13. Cant NW, Liu IOY, Patterson MJ (2006) J Catal 243:309
14. Urakawa A, Baiker A, in preparation
15. Nova I, Lietti L, Forzatti P (2008) Catal Today 136:128
16. Mulla SS, Chaugule SS, Yezerets A, Currier NW, Delgass WN, Ribeiro FH (2008) Catal Today 136:136
17. Maeda N, Urakawa A, Baiker A, submitted for publication
18. Ji Y, Choi J-S, Toops TJ, Crocker M, Naseri M (2008) Catal Today 136:146
19. Ji YY, Toops TJ, Crocker M (2007) Catal Lett 119:257
20. Desikusumastuti A, Staudt T, Grönbeck H, Libuda J (2008) J Catal 255:127
21. Nova I, Castoldi L, Prinetto F, Dal Santo V, Lietti L, Tronconi E, Forzatti P, Ghiotti G, Psaro R, Recchia S (2004) Top Catal 30–31:181
22. Cheol-Woo Y, Ja Hun K, Szanyi J (2007) J Phys Chem C 111:15299
23. Kato R, Rolfe J (1967) J Chem Phys 47:1901
24. Fanson PT, Horton MR, Delgass WN, Lauterbach J (2003) Appl Catal B 46:393
25. Narayanamurti V, Seward WD, Pohl RO (1966) Phys Rev 148:481
26. Taha S, Tosson M (1994) Thermochim Acta 236:217
27. Nova I, Castoldi L, Lietti L, Tronconi E, Forzatti P, Prinetto F, Ghiotti G (2004) J Catal 222:377
28. Luo J-Y, Meng M, Li X-G, Zha Y-Q (2008) Micropor Mesopor Mater 113:277